DOI: 10.13009/EUCASS2017-241

On the effect of axial turbine rotor blade design on efficiency: a parametric study of the Baljé-diagram

Louis Souverein, Lucrezia Veggi+, Samuel Sudhof§*
Roland Behr, Oskar Haidn+*
** Ariane Group, 81633 Munich, Germany*
+ Technical University of Munich, 85748 Garching, Germany
§ DLR Institut für Raumfahrtantriebe, 74239 Hardthausen, Germany
Corresponding author: louis.souverein@airbusafran-launchers.com

Abstract
For the preliminary design of a turbomachine, it is imperative to have an approach for estimating the machine characteristics based on the machine specifications. One convenient approach is based on the Baljé-Diagram. Necessarily, certain assumptions need to be made, including the use of semi-empirical relations for efficiencies. The motivation for the current work is to investigate the range in which the blade efficiency might vary based on a parametric study, including CFD simulations for four different blade profiling approaches and five design cases. The impact on the overall machine stage efficiency will be verified.

List of symbols

a^*	Cutter diameter [m]
c_0	Spouting velocity [m/s]
c	Absolute velocity [m/s]
C	Blade chord [m]
C_p	Specific heat, constant pressure [J/kg/K]
C_p	Pressure coefficient [-]
D	Outer diameter of the rotor [m]
D_s	Specific diameter [-]
g_0	Gravitational acceleration, $g_0=9.81$ [m²/s]
h	Blade height [m]
H	Specific work [m²/s²]
i	Incidence angle [°]
N	Rotation rate [rpm]
N_s	Specific rotational speed [-]
p	Pressure [bar]
P	Power [kW]
r	Radius [m]
t	Blade pitch [m]
T	Temperature [K]
u	Rotor circumferential center line velocity [m/s]
V	Volumetric flow rate [m³/s]
w	Relative velocity [m/s]
x,y	Axial, circumferential coordinate [mm]
Y'	Pressure loss coefficient [-]
Z	Number of blades [-]
α	Absolute angle [°]
β	Relative angle [°]
β_w^*	Wheel-disk friction coefficient [-]
δ	Deviation angle [°]
$\Delta\beta$	Wedge angle [°]
γ	Ratio of specific heats [-]
Γ	Uncovered turning [°]
η	Efficiency [-]
θ	Turning angle $\theta = 180- \beta_2- \beta_3$ [°]
Ψ	Zweifel number
Ψ_N, Ψ_R	Stator and rotor loss coefficients [-]

List of subscripts

ad	Adiabatic
des	Design
hyd	Hydraulic
LE	Leading edge
r	Relative
R	Rotor
s	Static
S	Stator
t	Total
TE	Trailing edge
u,m	Circumferential, meridional velocity components
1,2,3	Inlet stator, inlet rotor, outlet rotor

Copyright © 2017 by L. Souverein, L. Veggi and S. Sudhof. Published by the EUCASS association with permission.

DOI: 10.13009/EUCASS2017-241

1 Introduction

Similarity considerations show that four parameters are required to completely describe a turbomachine: the Reynolds number, the Mach number and two velocity ratios. These last two parameters can be expressed in terms of a specific rotational speed *Ns* and specific diameter *Ds* to be conveniently represented in a single diagram with iso-contours of efficiency, as described by Baljé in [1], see Figure 1 below. Often, it is taken 'as-is' without considering the underlying assumptions and empirical correlations. Actually, the diagram provides a 1-D design approach and it varies depending on the type of machine that is considered, being subject to geometrical similarity and the state of the art for the loss correlations. The current paper provides an investigation of the interrelation between geometry and losses. It investigates the effect of the blade design on the shape of the Baljé-diagram and the optimum performance. This is done for single stage low Mach number axial impulse turbines (vanishing reaction rate) consistent with the original Baljé diagram from [1].

A parametric study is performed, making turbine blade designs for several combinations of the non-dimensional rotation rate and diameter considering four different blade design approaches. The first method uses catalogue airfoils, which were investigated as an alternative for the design case in Souverein et al. [2]. The operational conditions from [2] are used as a baseline for the current study. The second method employs circular arcs to generate impulse blades as implicitly assumed by Baljé for the diagrams in his publication [1]. The third profiling approach is based on Aungier [3] and uses polynomial segments to describe the blades. Finally, the fourth method applies rational Bézier curves to define the blade profiles. All parametric designs are analysed with computational fluid dynamical (CFD) simulations to verify the rotor efficiency prediction from Baljé [1]. In addition, the relation between efficiency and flow topology is investigated. Based on these results, the turbine hydraulic efficiency can be increased by 10% compared to the Baljé prediction, depending on the blade design.

2 Theoretical background

As described in [1], it can be shown by means of the Buckingham π-theory that four parameters are required to completely describe a turbomachine: the Reynolds number, the Mach number, the specific rotational speed *Ns* and the specific diameter *Ds*. Alternatively, the definitions of *Ns* and *Ds* can be derived quite elegantly by defining a standard turbine (subscript "*s*") with $V_{3,s} \equiv 1$ and $H_{ad,s} \equiv 1$ and by observing that:

$$V_3 \propto ND^3 \qquad \text{and} \qquad H_{ad} \propto N^2D^2 \tag{1}$$

One can compare the volumetric flow rate and the specific work to that of the standard turbine as follows:

$$\frac{V_3}{V_{3,s}} = \frac{ND^3}{N_sD_s^3} \qquad \text{and} \qquad \frac{H_{ad}}{H_{ad,s}} = \frac{N^2D^2}{N_s^2D_s^2} \tag{2}$$

Rewriting both equations yields:

$$N_s = \frac{NV_3^{1/2}}{\left(\frac{H_{ad}}{g_0}\right)^{3/4}} \qquad \text{and} \qquad D_s = \frac{D\left(\frac{H_{ad}}{g_0}\right)^{1/4}}{V_3^{1/2}} \tag{3}$$

Ns and *Ds* are hence nothing more than the rotation rate and diameter of the standard turbine with unit volumetric flow rate and specific work. They can also be written [1] in truly non-dimensional form, but this paper will use the same definition as used in the diagram shown in [1] for consistency. For the main reason, the constant g_0 is added since Baljé uses Imperial units and defines *H* as the head in *feet* rather than the specific work in m^2/s^2. The equations remain valid for any system of units and definition of *Ns* and *Ds*, although the numerical values may change. It is noted that the outer rotor diameter is used in all derivations. The numerical subscripts refer to stator inlet (*1*), rotor inlet (*2*) and rotor outlet (*3*). With the definition of the spouting velocity c_0, it can be observed that another commonly used quantity for characterizing turbomachines u/c_0 is proportional to the product of *Ns* and *Ds*, effectively losing one degree of freedom:

$$c_0 = \sqrt{2H_{ad}} = \sqrt{2C_pT_{t1}\left(1-\left(\frac{p_{s3}}{p_{t1}}\right)^{\frac{\gamma-1}{\gamma}}\right)} \qquad \text{and} \qquad u \propto ND$$
$$N_sD_s = \frac{ND}{H_{ad}^{1/2}} \propto \frac{u}{c_0} \tag{4}$$

DOI: 10.13009/EUCASS2017-241

The Baljé-diagram directly relates the *Ns* and *Ds* to the turbine efficiency. Using the equations in [1], the diagram has been reproduced for the current investigation, see Figure 1 (red concentric iso-contours: efficiency η; cyan iso-contours: rotor loss coefficient Ψ_R). The details of the derivation will not be repeated, but a few relevant points will be highlighted here.

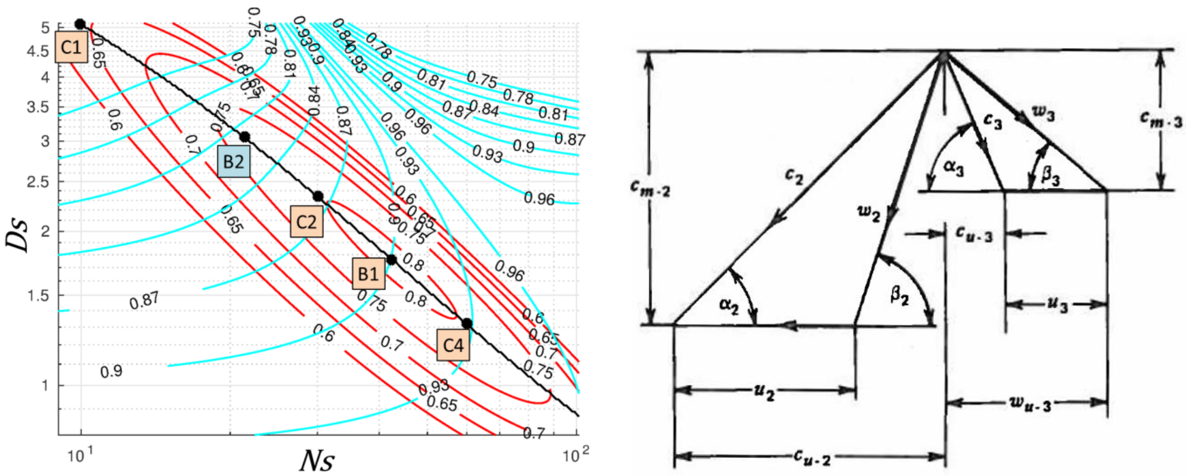

Figure 1: Baljé-diagram reproduced using Eq. 6 and Eq. 7 (left) and definition of velocity triangles [4] (right)

The Baljé-diagram derives directly from Euler's turbomachinery equation (conservation of impulse), using blade loss coefficients for stator and rotor to relate the circumferential velocity components to the ideal velocity that could be obtained for loss free flow. The blade loss coefficients and efficiencies are defined by (see [1] and [5]):

$$\psi_N = \frac{c_2}{c_{2,ad}} = \sqrt{\eta_S} \quad \text{and} \quad \psi_R = \frac{w_3}{w_{3,ad}} = \sqrt{\eta_R}$$

$$c_{2,ad} = \sqrt{2C_pT_{t1}\left(1-\left(\frac{p_{s2}}{p_{t1}}\right)^{\frac{\gamma-1}{\gamma}}\right)} \quad \text{and} \quad w_{3,ad} = \sqrt{2C_pT_{rt2}\left(1-\left(\frac{p_{s3}}{p_{rt2}}\right)^{\frac{\gamma-1}{\gamma}}\right)} \qquad \textbf{(5)}$$

Baljé states [1] that the stator loss coefficient varies little and sets it to Ψ_N = 0.96. For the current reference case [2], this value was indeed found to be appropriate. For the rotor loss coefficient Ψ_R, a semi-empirical dependence on the blade inlet angle and aspect ratio is proposed in [1]:

$$\Psi_N = 0.96 \quad \text{and} \quad \Psi_R = \left[1 - 0.228\left(1-\frac{\beta_2}{90}\right)^3\right]\left[1-0.06\frac{c}{h}\right] \qquad \textbf{(6)}$$

Applying the proper algebra, the turbine efficiency can be expressed completely in terms of *Ns*, *Ds*, the reaction rate, the absolute stator exit angle and both blade loss coefficients. Furthermore, the equation can be supplemented to correct for additional loss terms, such as the wheel-disk side friction that is included in [1]. Assuming zero reaction (impulse turbine), the equation can be simplified to its final form used to generate the diagram in Figure 1:

$$\eta = \frac{N_sD_s\sqrt{1-2\frac{h}{D}+2\left(\frac{h}{D}\right)^2}}{77}[1+\psi_R]\left\{\psi_N\cos\alpha_2 - \frac{N_sD_s\sqrt{1-2\frac{h}{D}+2\left(\frac{h}{D}\right)^2}}{154}\right\} - \frac{N_s^3D_s^5 16\beta_w^*\left(1-2\frac{h}{D}\right)^5}{154^3} \qquad \textbf{(7)}$$

The factor *h/D* appears, since *Ds* is defined at the rotor tip whereas the velocity triangles for Euler's turbomachinery equation are defined at the centre stream line. The value of the wheel-disk side friction coefficient is $\beta_w^* = 3 \times 10^{-3}$ for large Reynolds numbers.

Figure 2 shows the effect of different parameters on the shape of the Baljé-diagram, based on Eq. 6 and Eq. 7. Starting from the first panel on the left, the limits of the efficiency iso-contours are compared to the ideal case with $\Psi_N=1$, $\Psi_R=1$ and without disk side friction. The "geometrical limit" corresponds to $h=D/2$ – for smaller *Ds*, the blade height exceeds the disk radius, which is geometrically impossible. The "energy limit" corresponds to $u/c_0=1$, since the tip speed physically cannot exceed the spouting velocity for a turbine. Both the correlation for Ψ_R (Eq. 6) and the disk side friction in Eq. 7 have the effect of closing the Baljé-diagram compared to the ideal case. The geometrical assumptions and loss coefficients hence only affect the "loss limit" and impose an upper limit for the optimal Ds. The second and third panel show the effect of Ψ_N and Ψ_R for homogeneous constant values of both parameters compared to the values from Eq. 6. Indeed, Ψ_N only has a minor effect on the diagram whereas Ψ_R has a significant influence.

DOI: 10.13009/EUCASS2017-241

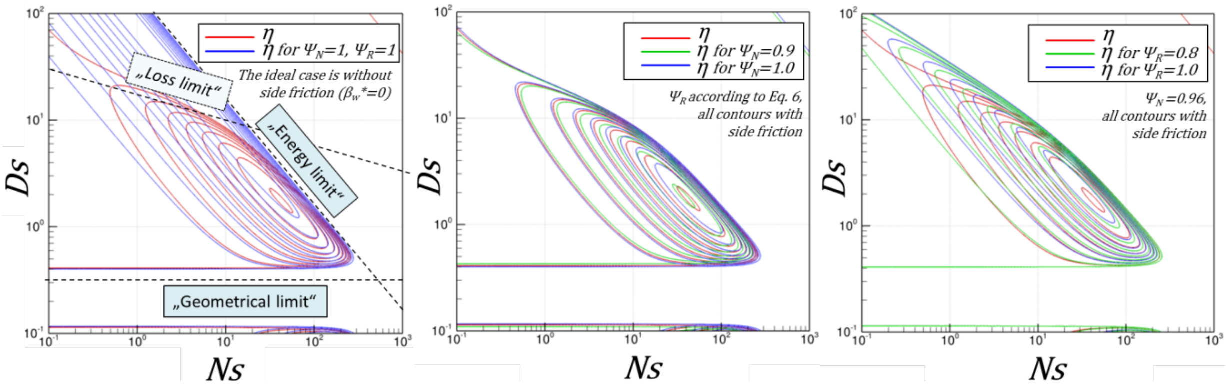

Figure 2: Effect of different parameters on the shape of the Baljé-diagram

Looking at the equations presented above, the semi-empirical element of the otherwise theoretical equation for the Baljé-diagram resides in the loss coefficients. As will be shown below, the effect of the disk friction is limited to a few percent for designs close to the optimum line. Assuming that the stator loss coefficient Ψ_N shows indeed little variation and provided that it has little impact on the diagram, this leaves its rotor homologue Ψ_R as a major driving factor for the turbine efficiency. It hence incorporates a major part of the assumption of "geometrical similarity". The effect of the rotor blade geometry on Ψ_R and the turbine efficiency is therefore the central topic of this paper.
The rotor loss coefficient's variability has been evaluated for four blade profiling approaches, defining several design cases on the optimum line of maximum efficiency in the Baljé-diagram, as shown in Figure 1 and Table 1. Noteworthy is that the *Ns* and Ds values for case B2 corresponds to the conceptual 120kN TP-LOX axial turbine design from [2]. Case B1 constitutes the point of the global maximum efficiency in the Baljé-diagram.

Blade design case	**C1**	**B2**	**C2**	**B1**	**C4**
Specific speed - Baljé, *Ns*	10	20.7	30	42.3	60
Specific diameter - Baljé, *Ds*	5.1	3.0	2.3	1.8	1.3

Table 1: Blade design cases

3 Considered blade design approaches

This section describes the four blade design approaches that were employed during the current investigation.

3.1 Catalogue blading

Catalogue blade profiles were investigated as an alternative for the design case from [2], which serves as the reference for the current investigation. The main advantage of this method is that the profile characteristics are known and well documented. On the other hand, the blade geometries are not parametrized and the approach depends on the availability of a profile that fits the design needs. The selection of a suitable blade profile is based on appropriate ranges of tabulated inlet/outlet angles and the Mach number range, see [6]. Based on the empirical correlations provided for each profile, the required blade pitch and stagger angle are deduced.

3.2 Circular arc blading

A straightforward way of parametrizing a blade profile from manufacturing point of view is by means of circular arcs. The pressure surface of the blade consists of a single arc with radius r_2, see Figure 3. At the leading edge and trailing edge, the gradient of the arc is equal to the desired blade angle. The suction side is defined by two linear line segments starting with the same gradient as the suction surface arc. Both segments are joined by a circular arc of radius r_1. In the most general case, the blade can be given a stagger angle, and arc having different centres, see for example Douglas [7]. In the specific case considered here, both arcs r_1 and r_2 are concentric and the blade has no stagger angle. The resulting impulse blade profile has equal inlet and outlet blade angles and a constant blade passage width a^* (the "cutter diameter"). The number of blades is directly determined by the value of a^*, the blade angle and the rotor diameter:

$$N = \pi D sin\beta_2 / a^* \quad \textbf{(8)}$$

DOI: 10.13009/EUCASS2017-241

This type of blading satisfies the assumption made by Baljé [1] to relate the impulse blade aspect ratio *h/C* in the semi-empirical equation for the rotor blade loss coefficient Ψ_R (Eq. 6) to the blade angle and the blade height:

$$\frac{C}{h} = \frac{4cos\beta_2 a^*/D}{h/D} \quad \textbf{(9)}$$

Effectively, this assumption relates the blade chord to the "cutter diameter": $C = 4cos\beta_2 a^*$. Hence, for a given blade angle, the complete blade geometry is defined by the value of a^*, which is taken equal to $a^* = 0.01$ in [1]. As stated before, this assumption, together with Eq. (6) constitutes the main condition for "geometrical similarity" underlying Figure 1. It is the reference case for the parametric study of the Baljé diagram.

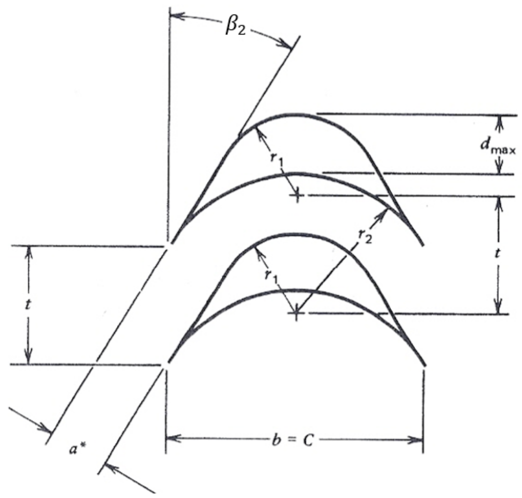

Figure 3: Circular arc blading: geometrical parameters

3.3 Polynomial blading

This airfoil design is based on an approach described by Aungier [3] which defines the profile surfaces on the pressure and suction side by means of polynomial segments. To fullfill the desired turning requirements for the blade row, empirical correlations are used to relate the inlet and exit velocity triangles from the preliminary designto basic geometrical parameters such as the inlet and exit blade angles, pitch-to-chord length ratio, blade numbers, stagger angle, throat-to-pitch ratio, axial chord and inlet height. The uncovered turning Γ has to be specified in order to complete the airfoil definition. The basic geometrical parameters defining the profile shape are summarized in Figure 4.

The pressure and the suction side of the airfoil are described by a series of third-order polynomials connecting adjacent defining points. To obtain continuous surface curvatures, the first and second derivatives must be matched at each defining point. The coordinates of the points on the surfaces are determined by the geometrical parameters obtained before. A minimum of three basic points is required on the suction surface, with the possibility to extend the number of defining points to five in order to better specify the shape of the surface. Similarly, two points are mandatory on the pressure side for the definition of the surface, and an additional two points are optional. The polynomial segments between the defining points have the following general form:

$$y_j = a_{j,1} + a_{j,2}z + a_{j,3}z^2 + a_{j,4}z^3 \quad \textbf{(10)}$$

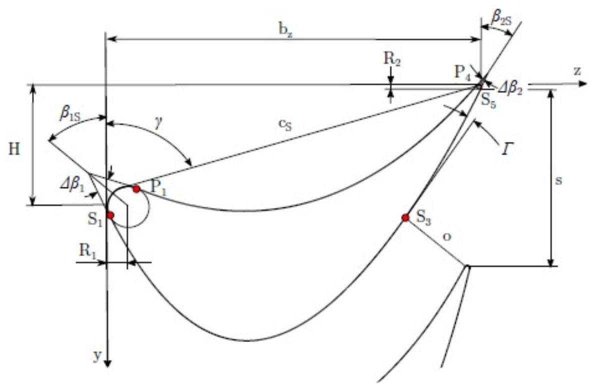

Figure 4: Polynomial blading: geometrical parameters

where j is the curve number. If one side of the airfoil is defined by two points, then one single polynomial segment describes the surface. Accordingly, with three defining points the surface will have two polynomial segments.

To determine the polynomial coefficients, it is necessary to solve four equations for each curve. The equations are obtained by requiring continuous derivatives at the defining points, which leads to a dependency of the polynomial coefficients of adjacent curves. The polynomial coefficients are determined by solving the resulting matrix equation:

$$[A] = [C]^{-1}[B]^T \quad \textbf{(11)}$$

The matrix $[A]$ contains N polynomial coefficients, where $N = 4N_c$ with N_c is the number of curves describing both side of the airfoil. The matrix $[B]$ contains N match point conditions and $[C]$ is a $N \times N$ matrix containing the defining equations.

The leading and trailing edge are assumed to be circular arcs matching the pressure and suction surfaces at their end points. For the complete definition of each arc, nose radii and wedge angles are supplied. For the evaluation of the airfoil design, one significant feature is the passage width distribution from inlet to outlet of the blade row. For a reaction turbine, the passage width should generally be monotonically decreasing, with a flatter distribution for smaller the reaction rates. For a vanishing reaction rate (approaching zero) the passage width should be constant from inlet to discharge.

DOI: 10.13009/EUCASS2017-241

Since the design approaches are partly complementary, the values obtained from Baljé [1] have been used for the current investigation wherever applicable, in view of the objective of maintaining geometrical similarity (e.g. for *C/h*, blade number, stagger angle), For the parameters that are specific to the polynomial blading approach, settings were found that provide a suitable profile shape for all all cases, see Table 2.

Incidence angle	i [deg]	4
Deviation angle	δ [deg]	0
Wedge angle at LE	$\Delta\beta_{LE}$ [deg]	15
Wedge angle at TE	$\Delta\beta_{TE}$ [deg]	10
Uncovered turning	Γ [deg]	14

Table 2: Polynomial blading specific settings

3.4 Bézier blading

The Bézier blading method described hereafter was developed to generate blades as tensor product NURBS surfaces. To maintain comparability with the original Baljé approach, the profile is prismatic for this exercise, although the method is not limited to such cases. It contains a rule set which is the same for all profiles and a parameter set that is varied between the profiles. The rules used for this task are similar to the ones used for the polynomial blades described above, because this method is based on the same paper by Pritchard [8] that also inspired Aungier's [3] method. The four defining points at the leading and trailing edges as well as the one at the throat are in this rule set as well. The suction and pressure side arcs are third degree rational Bézier curves instead of third degree polynomial function graphs, see Figure 5.

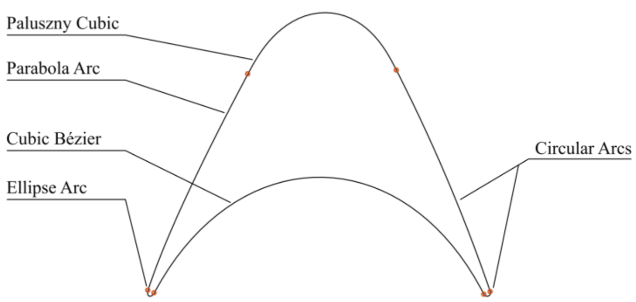

Figure 5: Segment curves of the Bézier profiles

Bézier curves have useful proven geometric properties relating to the control points which define their shape. One of these properties is the variation diminishing property, which states that no line can intersect the Bézier curve more often than it intersects the polygon formed by connecting the control points with straight lines (i.e. the control polygon) [9]. This property can be used to mathematically rule out the existence of inflection points on a curve, which plague Pritchard's profiles [8], by proper choice of control points through the rule set. A third order (cubic) rational Bézier curve possesses the desired number of degrees of freedom to ensure curvature continuity (i.e. G2) and form a fair curve at the same time [10]. Paluszny et al. [10] parametrized these curves in a way that leaves two degrees of freedom open to control the curve shape. Although Paluszny et al. do not name the parameters, the terms "pointedness" and "left/right bias" give a reasonable description of how the parameters influence the shape of the resulting curve.

In this special case of a pure impulse blade with large allowable turning angles, a subdivision of the suction side into a total of three segments yielded the necessary control over the curve: A circular arc of uncovered turning, the Paluszny cubic, and a parabola arc that connects (G2) with the Paluszny cubic at the inlet, in a fashion that is equivalent to the arc of uncovered turning at the outlet. The pressure side is shaped to generate an approximately linearly converging passage by fitting the pressure side to a normal projection of the suction side. Lastly, the leading edge was changed from Pritchard's circular arc to an elliptical edge. The specified leading edge radius was interpreted as the minor half-axis, which means that an additional eccentricity parameter resulted. In this study, it is constant 0.80. The trailing edge remained as a circular arc. The open parameters for this design method are the angle of uncovered turning, the leading edge wedge angle and the pointedness and bias parameter of the suction side Paluszny cubic, see Table 3.

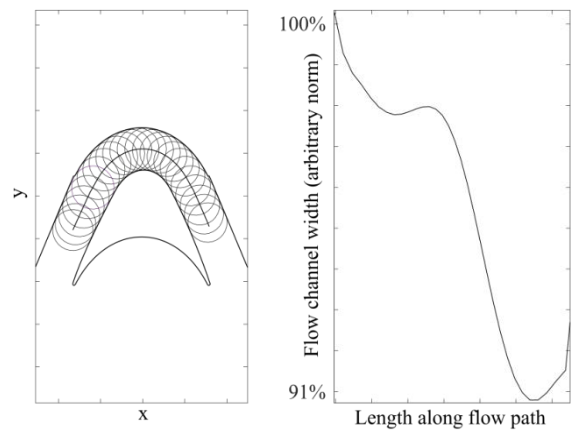

Figure 6: Channel width analysis

The choice of parameters followed guidelines, rather than precise rules. Under the assumption that a smaller outlet angle carries a higher risk of flow separation at the uncovered turning, the angle of uncovered turning is lower in more highly loaded profiles. The inlet wedge angle was selected somewhat higher than the uncovered turning, since this allows for a slightly convergent channel shape

DOI: 10.13009/EUCASS2017-241

throughout. A largest circle distance measure determined the channel width at 100 points along the profile (see Figure 6), to verify that the choice of angles led to a well-formed channel.
A major point in profile design is the suction side curve, and especially the distribution of curvature on it [11]. The Paluszny cubic was shaped in an interactive program with several criteria in mind. The curvature derivative should not have pronounced extrema (spikes), as they are akin to curvature discontinuities which can cause flow separation. If possible while maintaining this criterion, the bias parameter was chosen so that the maximum in curvature lies slightly towards the inlet. If the criteria above can be matched with more than one set of parameters, the parameter set with the lower bending energy was selected. Parameters were not revised with CFD results.

Blade design case	**C1**	**B2**	**C2**	**B1**	**C4**
Uncovered turning [deg]	6	6	8	12	11
Leading edge angle [deg]	8	8	10	14	13
Pointedness	0.298	0.38	0.432	0.473	0.524
Bias	-1.00	-1.28	-1.4	-1.49	-1.73

Table 3: Bézier blading specific settings

3.5 Comparison of designs

Using the Baljé-diagram, a design can be generated for each case defined in Table 1. The principal parameters are summarized in Table 4 (the definition of [7] was used for the Zweifel number). These values were kept fixed for all blade profiling approaches. The profile shape was kept constant along the height. In addition to the general parameters listed in Table 4, some general settings were used. The stagger angle for the catalogue blade is 80.2°, for all other blades it is 90°. The catalogue blade has a design reaction rate of 0.15, whereas all other blades were designed for vanishing reaction. The leading and trailing edge radii for all parametric blades were set to 1% of the chord, compared to 1.6% and 0.75% for the leading edge and the trailing edge of the catalogue blade respectively. The blade design was made before applying the rounding of the blade edges and hence the design value for the chord length differs from the effective value.
Only the reference case B2 was considered for the catalogue approach, since its design issues from the 120kN-study. Although it has the same *Ns* and *Ds* value as the B2-case, the design in [2] was generated using a different approach, following amongst others [12]. Hence, the values for the catalogue blade (listed in the column '120kN') differ from the values for the B2-case. Its rotor blade loss coefficient can however be estimated using Eq. 6, as can the resulting efficiency by means of Eq. 7. It will serve as a reference for the other designs at the same *Ns* and *Ds* (case B2).
The three parametric approaches each handled the problem of generating specific profiles for the cases in Table 1 individually. While the Baljé approach needed no additional parameters, the polynomial approach used CFD results to determine a set of parameters that were kept constant for all cases without adjustments. Lastly, the Bézier approach used a set of guidelines that were used to generate parameters individually for each of the cases. For the last each of the methods, better profiles may be possible if the respective restrictions were lifted. However, the purpose of this work is not the study of parameter optimization.
Figure 7 compares all blade profiles considered in this investigation. Generally, the blade profile becomes flatter (smaller turning angle) and the aspect ratio increases (larger blade height relative to the chord – more slender blades) for increasing *Ns*-values. The smaller blade aspect ratio and the stagger angle are obvious for the catalogue blade. The suction surface sides of the polynomial and Bézier blades are of similar shape, whereas the circular arc blade has a smaller curvature here. On the pressure side, the polynomial blade has the largest curvature and the circular arc blade has the smallest curvature. It is noted that these are not general properties of each blade design method. As mentioned before, it was not strived to obtain the optimal profile shape for each case and other profiles might have been obtained with another set of constraints. These blades fulfil the design conditions defined by the Baljé-diagram and serve the purpose of verifying the range of variation of the rotor loss coefficient.

4 Analysis approach

As stated above, the Baljé-diagram provides a non-dimensional design approach. A dimensional flow case is defined to evaluate the applicability of the underlying rotor loss coefficient correlation, both for the generation of the dimensional blade geometry and for its analysis in CFX. The axial turbine driving the conceptual 120kN LOX-TP design in [2] serves as basis for the boundary conditions for the current investigation, see Table 5. These values were kept fixed for all cases. It is noted that the volumetric flow rate V_3 (see Eq. 3) and hence the mass flow rate and power vary from design to design.

DOI: 10.13009/EUCASS2017-241

Design specifications		120kN	C1	B2	C2	B1	C4
Specific rotation rate	Ns	20.7	10	20.7	30	42.3	60
Specific diameter	Ds	3.1	5.1	3.0	2.3	1.8	1.3
Predicted stator blade loss coefficient	Ψ_N [-]	0.96	0.95	0.95	0.95	0.95	0.95
Predicted rotor blade loss coefficient	Ψ_R [-]	0.80	0.67	0.82	0.86	0.90	0.93
Predicted efficiency	η [-]	0.76	0.63	0.75	0.78	0.79	0.78
Predicted efficiency, w/o side friction	η_{hyd} [-]	0.78	0.67	0.77	0.80	0.80	0.79
Predicted power	P [kW]	243	47	239	533	1068	2123
Predicted power, w/o side friction	P_{hyd} [kW]	249	50	246	545	1080	2135
Geometrical design parameters							
Number of blades	Z [-]	65	69	98	123	146	177
Blade height ratio	h/D [-]	0.033	0.011	0.025	0.036	0.055	0.083
Chord to height ratio, design	C_{des}/h [-]	1.97	3.54	1.51	1.03	0.65	0.40
Chord to height ratio, effective	C/h [-]	1.97	3.32	1.37	0.91	0.56	0.33
Solidity	t/C [-]	0.71	1.24	0.93	0.78	0.70	0.65
Absolute flow angle, inlet rotor	α_2 [deg]	9.9	8.4	10.9	12.7	14.9	18.1
Relative flow angle, inlet rotor	β_2 [deg]	20.1	12.7	18.2	23.0	27.7	34.2
Relative flow angle, outlet rotor	β_3 [deg]	16.4	12.7	18.2	23.0	27.7	34.2
Turning angle	θ [deg]	144	155	144	134	125	112
Zweifel number	Ψ [-]	0.70	1.05	1.07	1.09	1.10	1.11

Table 4: Geometrical parameters for all design cases

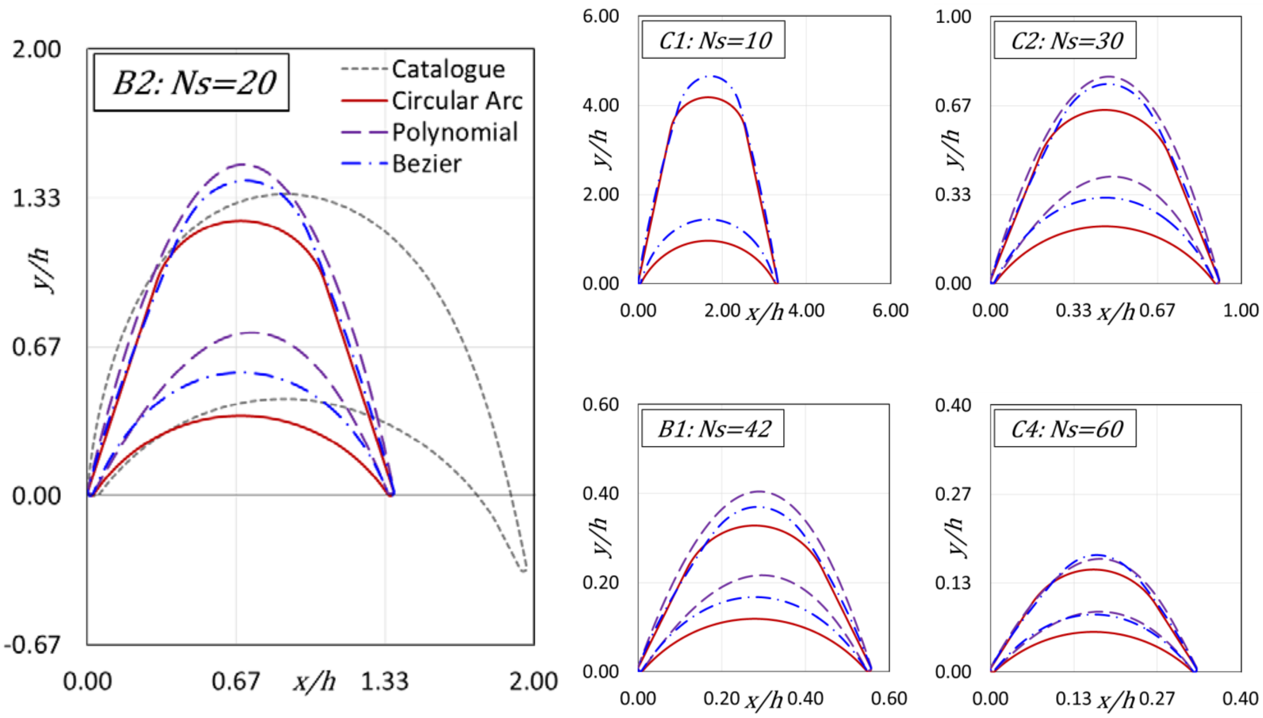

Figure 7: Overview of the investigated blade profile geometries

Rotation rate	**Total temperature turbine inlet**	**Total pressure turbine inlet**	**Total to static pressure ratio**	**Ideal specific work**
N = 25000 rpm	T_{t1} = 218 K	P_{t1} = 89 bar	P_{t1}/P_{s3} = 1.187	H_{ad} = 161844 m^2/s^2

Table 5: Design boundary conditions

DOI: 10.13009/EUCASS2017-241

For the CFX-simulations, the boundary conditions were based on Table 5. At the rotor inlet, total pressure and total temperature were set, assuming adiabatic flow through the stator. The total pressure at rotor inlet was set to a constant value of P_{t2} = *87.8bar* based on the 120kN data, resulting in a stator loss coefficient of Ψ_N = 0.95 compared to Ψ_N = 0.96 for the 120kN case, see Table 4. The slight discrepancy between both values is caused by the different absolute stator exit angle (and hence velocity c_2 and Ψ_N, see Eq. 5) in the Baljé design for the same boundary conditions. At the outlet, the design mass flow rate was prescribed. The effective total to static pressure ratio in the simulation depends on the efficiency. All simulations were made with para-hydrogen (real gas). The tables of the fluid properties were created with GASPAK.
The objective of this study is to evaluate the rotor blade efficiency for different design approaches. Therefore, the computational grid consists of only of the rotor domain. It has been verified for the 120kN case with catalogue blades from [2] that the results agree with the corresponding simulation including a stator when using the mixing plane approach. Figure 8 shows an example of an applied computational mesh for the 3D CFD simulations. The size of the computational grid depends on the geometry and on the design approach and varies from 0.5 to 1.5 million cells. The mesh was created using CFX-TurboGrid with the topology “single round round symmetric”. No tip clearance was implemented.

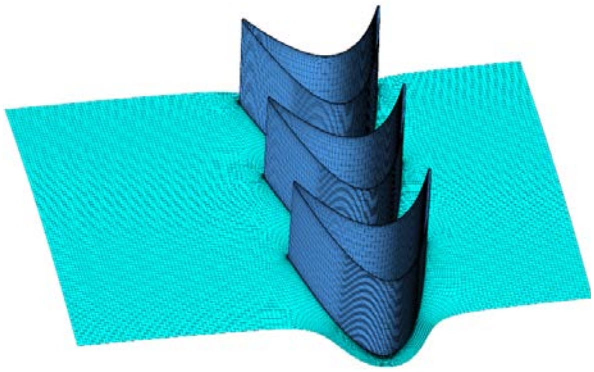

Figure 8: Example of a numerical mesh (polynomial blade, case B2)

One single passage has been simulated in steady state using rotational periodicity for the connection between the periodic boundaries. The standard SST model was used for modelling turbulence. All simulations were performed with the high resolution advection scheme. Only for the B2 case with the polynomial blading, the advection scheme was switched to “upwind” to obtain the desired convergence. All cases converged to O(1e-6) on the rms-residual.

5 Comparison of the flow fields

Prior to considering the integral performance quantities, the details of the flow field are compared for all design cases, with particular attention for the local loss generation as expressed by the relative total pressure and the relative Mach number to identify low momentum fluid regions. Finally, the pressure distribution and the velocity triangles are considered.
In the following plots, the relative total pressure has been normalised, as follows, using the definition of the pressure loss coefficient (see [5]):

$$\text{Pressure loss coefficient: } Y' = \frac{P_{tr2}-P_{tr3}}{P_{tr2}-P_3} \quad \rightarrow \quad \text{Relative total pressure normalization: } Y'_i = \frac{P_{tr2}-P_{tr,i}}{P_{tr2}-P_3} \qquad \textbf{(10)}$$

The values of P_{tr2} and P_3 are constants, area averaged over the complete channel outlet. $P_{tr,i}$ is the local total relative pressure in the flow field. Using this normalization of the total relative pressure, integrating Y'_i in the wake of the blade yields the loss coefficient Y', which in turn is approximately equal to *1*-Ψ_R. This enables a direct visual inspection of the locations in the flow field where the losses are generated, linking them to the blade loss coefficient Ψ_R. This interpretation of the total pressure is also consistent with the common approach of determining aerodynamic drag based on total pressure deficit in the wake survey method.

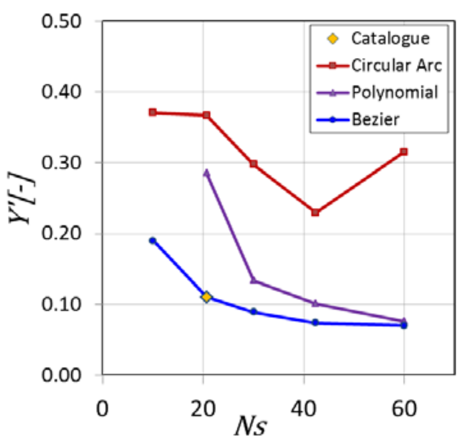

Figure 9: Pressure loss coefficient from CFD

The pressure loss coefficients for all blade designs are shown in Figure 9, with the effective Ns-values based on the simulation results plotted on the horizontal abscissa. The normalised relative total pressure Y'_i is shown in Figure 10 and Figure 11 for all blade designs. The view in the former figure concerns the flow field at 50% span in the blade-to-blade plane while the latter figure shows the flow topology in the channel outlet cross section 50% chord length downstream from the trailing edge. Note that for the polynomial blading, the “upwind” advection scheme was used for case B2 (see section 4). This most likely causes an overestimated of Y' by 0.05-0.07 points based on a comparison between “upwind” and “high resolution” for the other design cases. The

DOI: 10.13009/EUCASS2017-241

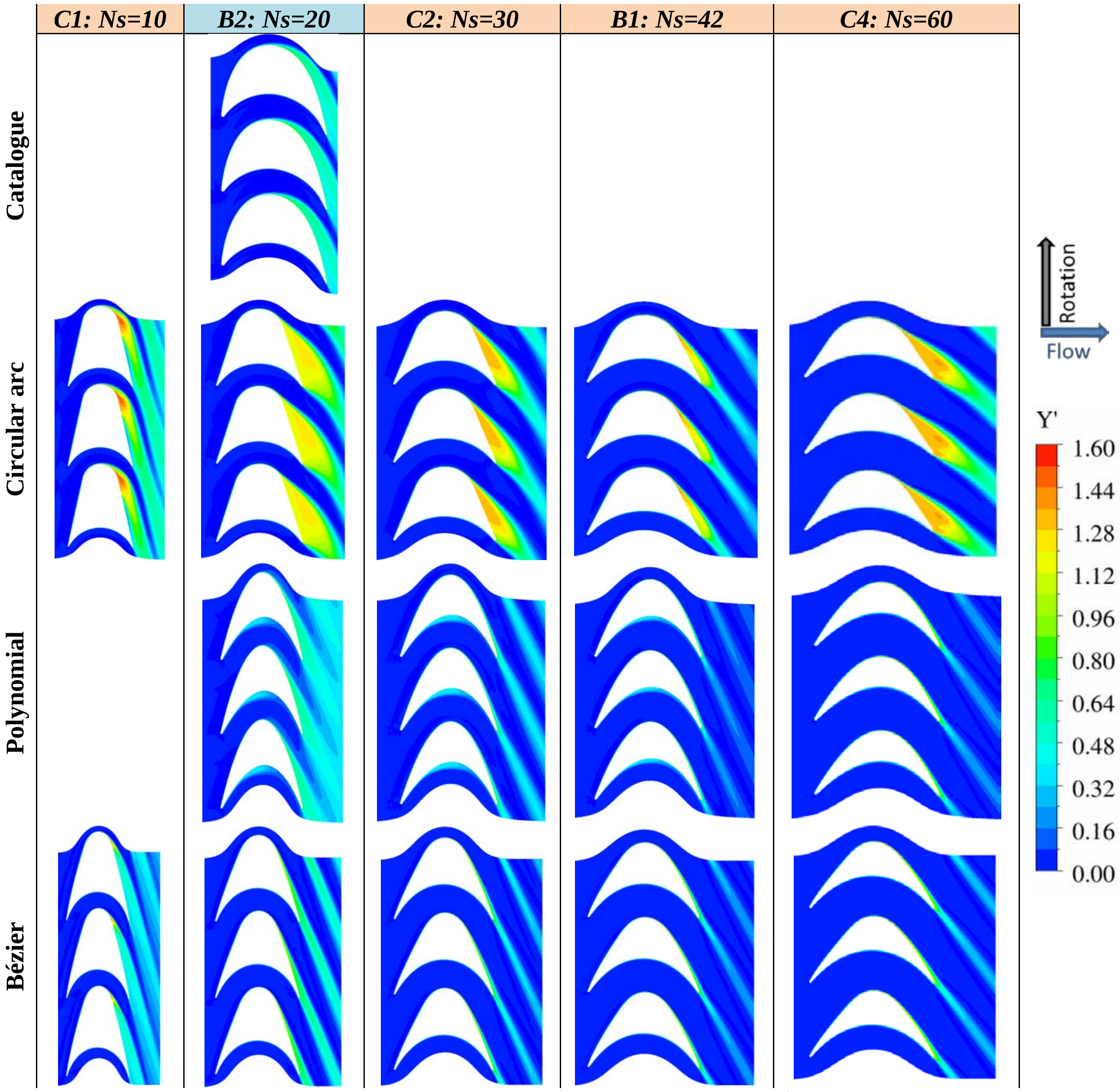

Figure 10: Blade-to-blade total pressure loss coefficient at 50% span (Y'_i as defined by Eq. 10)

effect of the advection scheme is also visible in Figure 10 and Figure 11, where the flow field for the downstream of the B2-polynomial blade appears to be smeared out compared to all other cases.

Considering Figure 9, the Bézier blading have the lowest losses for the current set of constraints, followed by the polynomial approach and the circular arc. The value for the catalogue profile is close to the Bézier blade for case B2. Looking at Figure 10 and Figure 11, the loss generation in the boundary layer and the subsequent blade wake are clearly visible. Avoiding flow separation or large low momentum regions is elemental for loss minimization, as a comparison between the contour plots and the integral values in Figure 9 confirms. The current circular arc designs are particularly affected, displaying large regions with high loss generation on the suction side starting from the downstream side on the transition point between arc and linear segment, where the change in blade curvature occurs. For the polynomial designs, higher loss regions occur on the pressure side for certain cases, also related to a low momentum region at the location of highest curvature. The catalogue blades display a relatively thick wake, but the total pressure losses are comparatively small.

The three-dimensional effects in the outlet flow field in Figure 11 depend in part on the blade design, but also show common aspects. For the small aspect ratio blades (small *Ns*), the blade wake completely fills the flow channel and

DOI: 10.13009/EUCASS2017-241

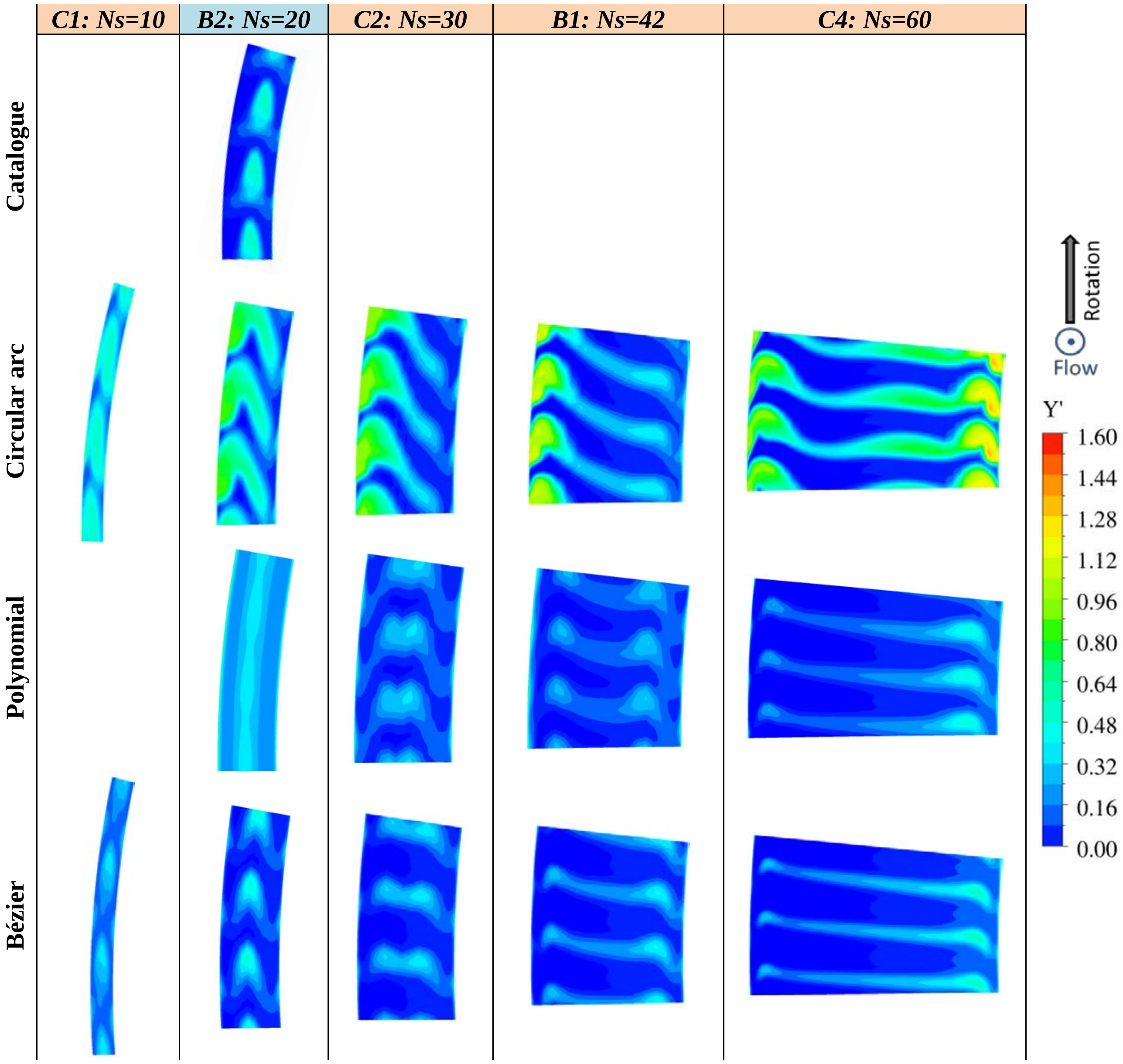

Figure 11: Outlet relative total pressure loss coefficient at 50% chord length downstream the trailing edge (Y'_i as defined by Eq. 10.)

the losses are mainly generated in the centre of the channel (mid-span). With increasing aspect ratio (larger Ns values), the losses appear to be generated mostly at the shroud and hub, although the most intense losses are generated at the shroud for the circular arc profiles at for cases B2, C2 and B1 (*Ns* = 20-42).

For the reference case B2, the Mach number iso-contours, the velocity triangles and the pressure coefficient distribution (blade loading) were considered in more detail, see Figure 12. The pressure coefficient is defined as:

$$c_p = \frac{p - p_2}{\frac{1}{2}\rho_2 w_2^2} \tag{11}$$

With p_2 respectively area averaged pressure and $1/2\,\rho_2 w_2^2$ the mass flow averaged dynamic pressure, both at rotor inlet. The pressure p is the local value on the blade surface.

The correlation between total relative pressure losses and low momentum region (low local Mach number) is visible for all blade designs. The catalogue blade has a lower overall Mach number due to the larger channel height and lower blade number, see Table 1, since the turbine design was made using a different approach. However, the range of variation of the Mach number is also smaller. This is also reflected in the pressure coefficient distribution (*Cp*), which shows only minimal changes over the full blade length, causing a homogeneous blade loading. The other blades all show a high Mach number on the suction side, corresponding to a peak in the pressure distribution.

DOI: 10.13009/EUCASS2017-241

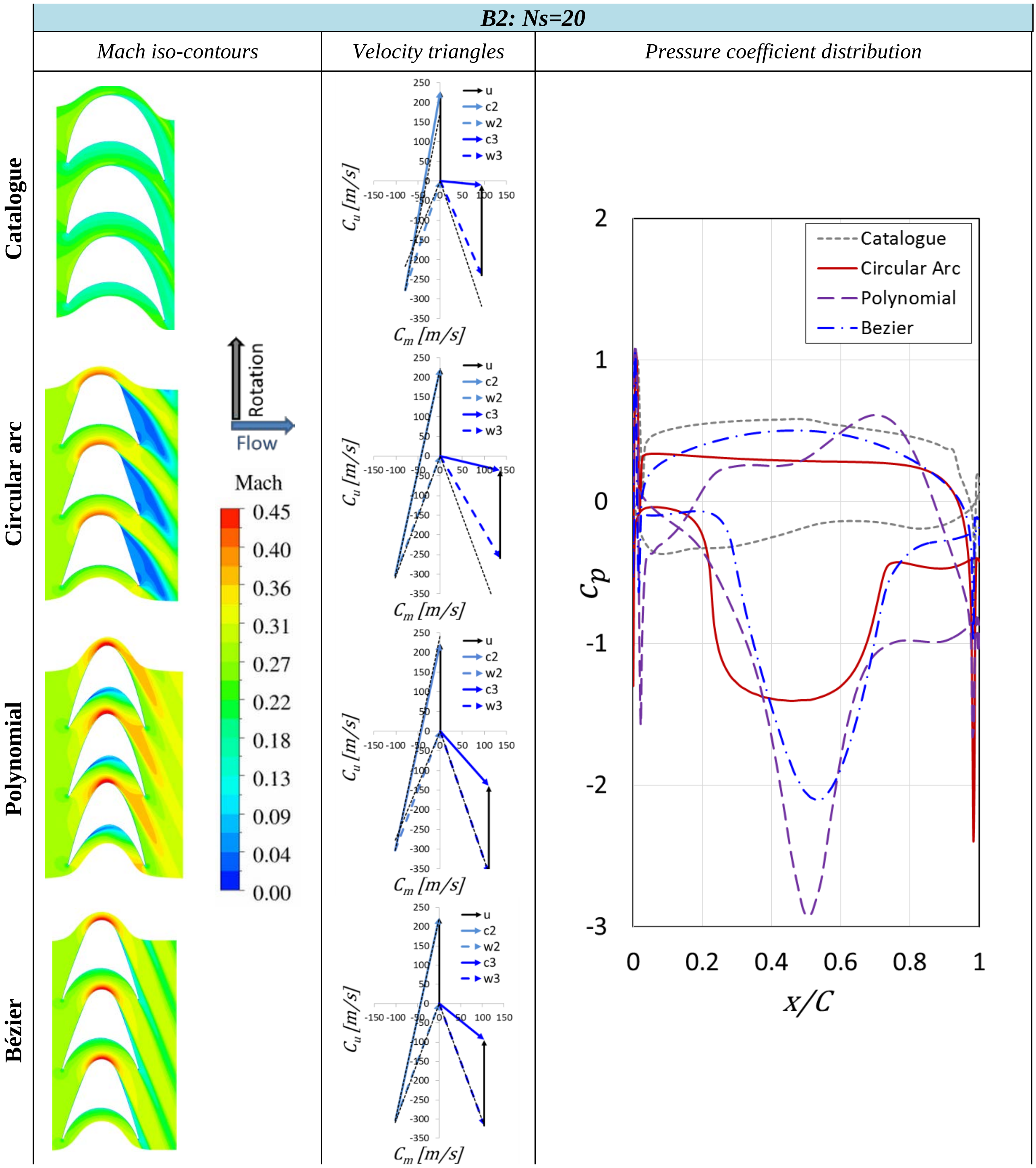

Figure 12: Detailed results for all blading types for case B2: *Ns*=20

However, the pressure loss coefficient for the Bézier blade and the catalogue profile are identical, notwithstanding the difference in pressure distribution, see Figure 9. The pressure peak is partly attributable to a smaller chord length of the parametric designs, which is taken from Eq. 9. Further, the parametric blades are designed to concentrate the turning in the guided channel, whereas the unguided parts of the catalogue design are loaded equally to the guided section.

The relation between curvature and pressure is clearly visible for the circular arc blading, with an almost discrete jump in the pressure distribution for each change in curvature. In all cases, the low momentum region is visible as a plateau in the *Cp*-distribution (in particular on the downstream suction side for all parametric blades and, and on the pressure side for the polynomial blade), which again is linked to the profile pressure drag.

DOI: 10.13009/EUCASS2017-241

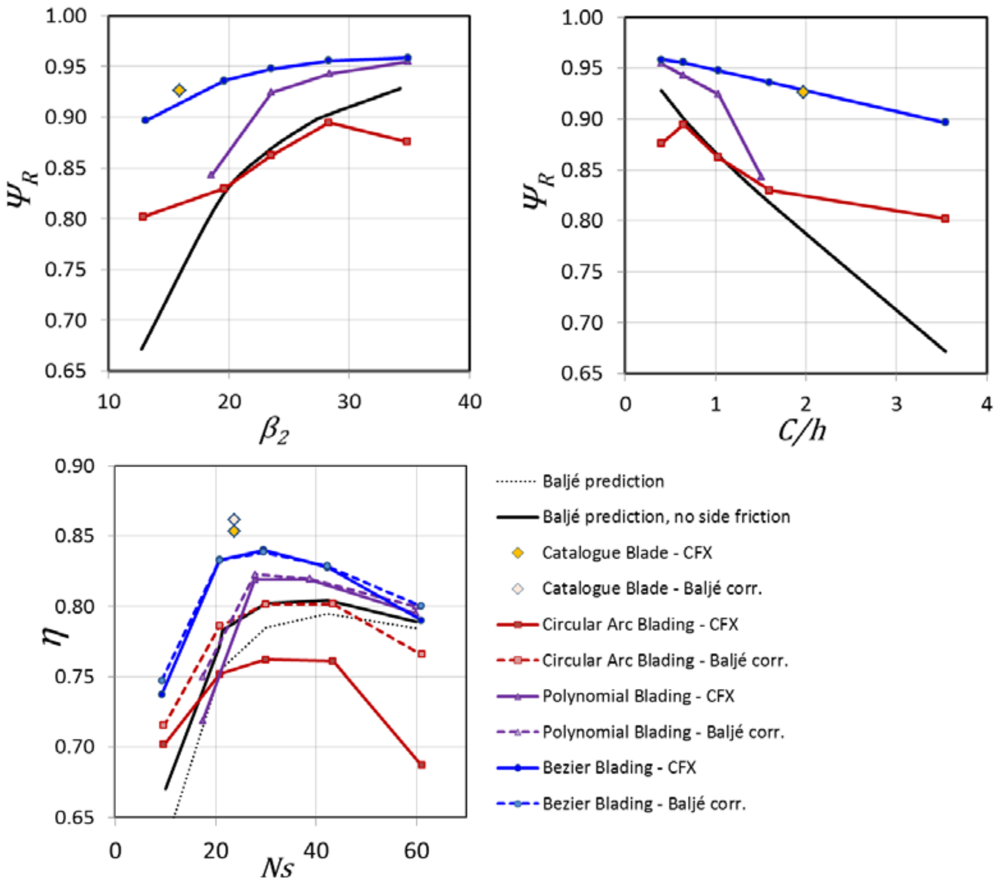

Figure 13: Rotor blade efficiency (top) and turbine efficiency results (bottom) comparison

The velocity triangles are mass flow averaged over the complete channel section at the inlet and outlet. The design blade angles are indicated by the black dashed lines. The catalogue profile and the circular arc blade show a relatively large deviation (velocity w_3), consistent with the low momentum region. In the case of the polynomial and Bézier blades, there is a very good agreement between the simulated flow angles and the blade angles, indicating low deviation.

6 Comparison of the rotor blade efficiency results

This section investigates the predictive power of both the rotor blade loss coefficient and the assumption of geometric similarity, which are defined in section 2. The loss coefficient Ψ_R has been computed from the simulation results presented in the previous section. It is plotted against the two geometrical parameters from Eq. 6 (the inlet blade angle β_2 and the chord to blade height ratioC/h) in the upper half of Figure 13 and compared to the Ψ_R-values based on the equation (the black curve). Note that the value of Ψ_R for the B2 polynomial case is most likely underestimated by about 0.03-0.04 points due to the use of the "upwind" advection scheme leading to an approx. 0.02 lower value for η, see also section 5.
The circular arc blades show a good agreement with the prediction for a range between Ns=20-42. However, there is also a general deviation from the curve shape proposed by Eq. 6. In this respect, the blades generated with the Polynomial and Bézier approaches show a generally higher than predicted efficiency with a good agreement in behaviour terms of the curve shape for the dependence on β_2 and C/h. The efficiency of the current catalogue blade design is similar to the Bézier profile. Generally, the values obtained with Eq. 6 appear to be conservative for the investigated case, being generally equal to or lower than CFD-predicted loss coefficients (with the exception of case C4 for the circular arc blade).
The lower half of Figure 13 compares the CFD-predicted efficiency to the prediction of Eq. 7. The pressure loss of the stator is accounted for by employing the total pressure at the stator inlet as reference pressure. The effect of side-friction is limited to a few percent, as is clear when comparing the dashed black line with the solid black line. Since the simulations do not include wheel-disk side friction, the solid line serves as reference for the current results. For

DOI: 10.13009/EUCASS2017-241

each case, the values obtained from the CFX-simulation are shown and compared with corrected Baljé-predictions that would have been obtained when using the simulation value for Ψ_R in Eq. 7 rather than the Ψ_R value from Eq. 6.
Comparing the solid lines with the simulation results, it is evident that even with the same design boundary conditions, a large variation in turbine efficiency is obtained (up to 10% between the circular arc and the Bézier designs, with the polynomial blading generally producing intermediate values). The catalogue profile displays the highest efficiency, although the results are not directly comparable since the blade has a higher chord length and smaller aspect ratio.
The comparison of the results for all blade designs shows the impact of the assumption of geometrical similarity on the efficiency prediction: there is a scatter of up to 5% in the corrected Baljé predictions (dashed lines for all blade cases), depending on the Ψ_R-value used. If the geometry dependence is accounted for by using the simulation value of Ψ_R for each individual blade profile, the deviation between Baljé-prediction and simulation is reduced to <1% for all design approaches except for the circular arc blades.
The reason for the deviation between simulation and corrected Baljé prediction for the circular arc blades is conjectured to be due to the large flow deviation induced by the significant low momentum blade wake. This causes an effective flow turning angle that is up to 15% below the design value from Baljé, see Figure 14, as was also observed from the velocity triangles in Figure 12. This violates the impulse blades assumption of equal inlet and outlet flow angles, causing the observed discrepancy. Indeed, the case for which the flow turning is best achieved (case C1) also shows the smallest deviation between predicted and effective efficiency in Figure 13.
For the polynomial, Bézier and catalogue blade design cases, the good agreement between the simulation value for the efficiency (which has been obtained from the effective power that is computed from the blade surface loads) and the prediction (which issues from the integral momentum balance) confirms the consistency of the results. It is an indication for soundness the equation and the assumptions underlying the Baljé-diagram.
In summary, the assumption of geometric similarity made in the derivation of the Baljé diagram is not a minor effect. For different viable rotor blade profiles that were all designed with the same geometrical parameters from Table 4, a variation of up to 10% in the efficiency was observed in the current investigation, depending on the details of the flow field. Using the appropriate values for the blade loss coefficients generally increases the accuracy of the Baljé prediction to within approx. 1%. The circular arc blades constitute the exception to this rule due to the large deviation from the design outlet flow angle that is not in line with the impulse blade assumption.

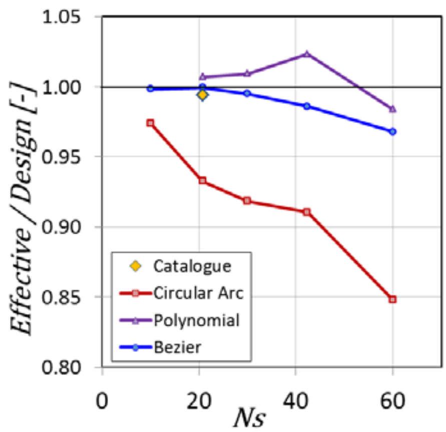

Figure 14: Turning angle: effective value (CFX) vs. design value (Baljé)

Conclusions

A parametric study has been performed within the Baljé diagram with the specific aim of investigating the impact of the blade design on the rotor loss coefficient and turbine efficiency. To this aim, three parametric blade profiling approaches have been used to generate designs, each fulfilling the geometrical boundary conditions prescribed by the original Baljé diagram as published in [1]. A fourth method, based on catalogue blades and an alternative turbine design approach, has been included as it provided the reference flow case in terms of physical boundary conditions. It is noted that more optimal designs and higher efficiencies might be achievable with each approach for another set of constraints.
Numerical simulations show that the rotor blade loss coefficient and the turbine efficiency depend strongly on the chosen profiling approach. The circular arc blade rotor loss coefficient agrees well with the Baljé correlation, although it deviates toward higher and lower Ns-values. For all other cases the efficiency is generally higher than the original prediction by Baljé. The highest efficiency is obtained with the catalog and Bézier profiles, the polynomial blades showing intermediate values. The variations could be linked in part to the flow field, specifically to low momentum regions resulting in a lower than expected flow turning angle.
The potential for increasing the rotor loss coefficient can be established through dedicated parametric studies, relaxing the geometric assumptions made in the derivation of the original Baljé diagram. In particular, the results indicate that the blade aspect ratio assumed in Baljé (see Eq. 9) might be too constraining in terms of flow turning, as

DOI: 10.13009/EUCASS2017-241

suggested by the strong peak in the loading of the parametric blades compared to the catalogue profile with larger chord length. Other “geometrical” factors that can be revisited include the blade number (affecting the passage width) and the reaction rate (which is included in the general equation for the Baljé diagram).
If appropriate blade loss coefficient correlations are used in the Baljé diagram, it has the potential of making accurate efficiency predictions. Since loss coefficients constitute the major semi-empirical element in the equations for the diagram, the otherwise theoretical equations provide an elegant way of making parameter studies for preliminary design. For the given data points, CFD results suggest that rotor loss coefficient can be increased by 5% and the turbine efficiencies can be increased by 10% compared to the original Baljé prediction depending on the blade design.

Acknowledgements

This work was performed within the national technology program TARES. This program is sponsored by the German Space Agency, DLR Bonn, under contract No. 50RL1210. The cooperation with the TU Munich took place within the frame of the Ludwig-Bölkow-Campus project KonRAT (LABAY83A), funded by the Bavarian Ministry of Economic Affairs and Media, Energy and Technology. The Bézier blading approach was developed at DLR Lampoldshausen and financed using their basic funding. All support is gratefully acknowledged. Finally, the contributions of Pierre Sivel, Timm Knapp and Andreas Ewald to the realisation of this work are gratefully acknowledged.

References

[1] O. E. Baljé, "A Study on Design Criteria and Matching of Turbomachines: Part A – Similarity Relations and Design Criteria of Turbines," *ASME Journal of Engineering for Power. Vol.84(1), pp..*, pp. 83-102, 1 Januar 1962.

[2] L. J. Souverein, C. Maeding, T. Aichner and M. Frey, "Design and tool anchoring for a 120kN expander cycle rocket engine LOX turbopump," in *6th EUCASS Conference*, Munich, 2015.

[3] R. H. Aungier, Turbine Aerodynamics, New York: ASME Press, 2006.

[4] O. E. Balje, Turbomachines: A Guide to Design, Selection and Theory, New York: John Wiley & Sons, Inc., 1981.

[5] A. Glassman, "Turbine Design and Application," NASA SP-290, 1994.

[6] M. Detj, G. Filippov and L. Lizariev, Atlas for turbine profiles, 1965.

[7] H. Douglas, "Liquid rocket engine turbines," NASA SP-8110, 1974.

[8] L. J. Pritchard, "An Eleven Parameter Axial Turbine Airfoil Geometry Model," in *Gas Turbine Conference and Exhibit*, Houst on, Texas, 1985.

[9] L. Piegel and W. Tiller, The NURBS Book, Heidelberg: Springer, 1997.

[10] M. Paluszny, F. Tovar and R. R. Patterson, "G2 composite cubic Bézier curves," *Journal of Computational and Applied Mathematics,* pp. 49-71, 15 February 1999.

[11] J. M. Anders, J. Haarmeyer and H. Heukenkamp, A parametric blade design system (Part I+ II), atech GmbH engineering software technology, 1999.

[12] A. Glassman, "Computer Code for Preliminary Sizing Analysis of Axial-Flow Turbines," NASA CR-4430, 1992.

[13] L. Fielding, Turbine Design, New York: ASME Press, 2000.

[14] M. Dejc and B. Trojanovskij, Untersuchung und Berechnung axialer Turbinenstufen, Berlin: VEB Verlag Technik, 1973.